Implementation and Evaluation of the Automated Model Reduction (AMORE) Version 1.1 Isoprene Oxidation Mechanism in GEOS-Chem

Benjamin Yang,[*ab] Forwood C. Wiser,[c] V. Faye McNeill,[bc] Arlene M. Fiore,[d] Madankui Tao,[abd] Daven K. Henze,[e] Siddhartha Sen,[f] and Daniel M. Westervelt[*a]

* Corresponding authors

[a] Lamont-Doherty Earth Observatory, Columbia University, Palisades, NY, USA
E-mail: benjamin.yang@columbia.edu, danielmw@ldeo.columbia.edu

[b] Department of Earth and Environmental Sciences, Columbia University, New York, NY, USA

[c] Department of Chemical Engineering, Columbia University, New York, NY, USA

[d] Department of Earth, Atmospheric, and Planetary Sciences, Massachusetts Institute of Technology, Cambridge, MA, USA

[e] Department of Mechanical Engineering, University of Colorado Boulder, Boulder, CO, USA

[f] Microsoft Research, New York, NY, USA

Table of Contents Entry

A chemical transport model with a graph theory-based isoprene oxidation mechanism is used to simulate ozone and secondary organic aerosol distributions needed to quantify health and climate impacts.

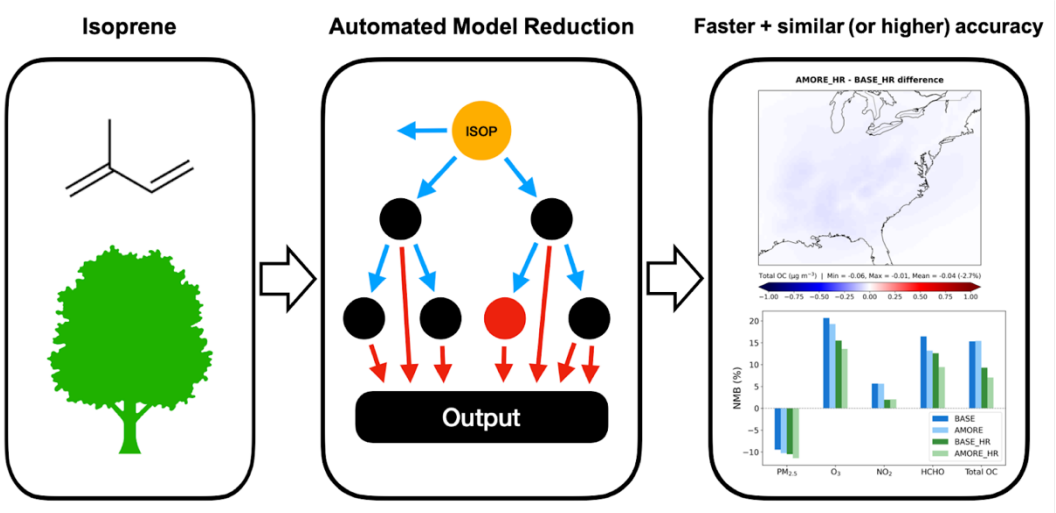

Abstract

Detailed chemical mechanisms are computationally challenging to include in large-scale chemical transport models such as GEOS-Chem. Employing a graph theory-based automated model reduction (AMORE) algorithm, we developed a new reduced (12 species and 23 reactions) gas-phase isoprene oxidation mechanism. We performed GEOS-Chem simulations for a full year (June 2018 – May 2019) with the default (BASE) and AMORE version 1.1 isoprene mechanisms at 2° × 2.5° horizontal resolution globally and 0.25° × 0.3125° resolution over the eastern United States (EUS). Additionally, we conducted BASE and AMORE sensitivity simulations in which biogenic isoprene and anthropogenic emissions were sequentially set to zero in the model. For the entire year simulated, GEOS-Chem was faster by 10% in total and 25% in the chemical solver (KPP) with the AMORE mechanism. Evaluating GEOS-Chem against surface observations from the Air Quality System (AQS) and Interagency Monitoring of Protected Visual Environments (IMPROVE) networks as well as satellite columns from the Tropospheric Monitoring Instrument (TROPOMI) and Cross-track Infrared Sounder (CrIS), our results show comparable accuracy in BASE and AMORE nested-grid simulations of air pollutants, with annual mean model bias changes of 1% for both $PM_{2.5}$ and O_3 over the EUS. From the sensitivity simulations, we find that US biogenic isoprene contributes to 7-9% of $PM_{2.5}$ and 3-4% of O_3 on average in summer over the EUS. This study indicates that AMORE is an attractive option for future GEOS-Chem modeling studies, especially where detailed isoprene chemistry is not the focus.

Environmental Significance

Atmospheric oxidation of isoprene leads to the secondary formation of air pollutants, namely fine particulate matter and ozone, which affect health and climate. The full isoprene oxidation mechanism is highly complex, involving hundreds of species and over a thousand reactions. To accurately and efficiently model atmospheric chemistry, the optimal balance between small mechanism size and accuracy should be achieved. We find that using our automated model reduction (AMORE) isoprene mechanism over the default mechanism in the GEOS-Chem chemical transport model not only speeds up simulations but also roughly maintains the accuracy of simulated air pollutant concentrations compared with surface and satellite-based observations. Our AMORE approach has the potential to be applied to other chemical mechanisms and models.

1. Introduction

Ambient fine particulate matter ($PM_{2.5}$) and ozone (O_3) were responsible for 4.14 million and 0.37 million global premature deaths, respectively, in 2019.[1] $PM_{2.5}$ is particularly harmful as these aerosols ≤ 2.5 μm in aerodynamic diameter can be inhaled deep into the lungs, and exposure to elevated $PM_{2.5}$ concentrations increases susceptibility to respiratory diseases such as asthma, lung cancer, and chronic obstructive pulmonary disease.[2] In addition, air quality is intricately linked with climate change. While O_3 exerts a net positive radiative forcing and aerosols induce either a negative or positive forcing, depending on the balance of scattering, absorption, and cloud interactions, climate change is expected to degrade air quality in polluted regions overall, involving changes in meteorology, deposition, and chemistry.[3] To better understand regional health impacts and climate feedbacks, we need to improve high-resolution modeled estimates of pollution not only directly emitted (primary) from anthropogenic and biogenic sources but also that formed through anthropogenic-biogenic chemical interactions (secondary).[4]

Isoprene (C_5H_8) is the predominant non-methane biogenic volatile organic compound (BVOC), representing about 50% of 1 Pg of total global annual BVOC emissions.[5] Most isoprene-emitting plant species are located in the humid tropics, and, in temperate regions, oak and aspen trees emit significant amounts of isoprene.[6] Monoterpenes and sesquiterpenes are other important BVOCs, constituting 15% and 3% of total global BVOC emissions.[5] The southeastern United States (US) is an extensively-studied isoprene hotspot with significant anthropogenic emissions. There, isoprene is primarily emitted during the warm, growing season and dominates hydroxyl radical (OH) reactivity in summer, while monoterpenes remain more constant and dominate O_3 and nitrate radical (NO_3) reactivity throughout the year.[7] In GEOS-Chem, isoprene is mostly oxidized by OH (85%), followed by O_3 (11%) and NO_3 (4%) pathways, over the southeastern US.[8]

Atmospheric photooxidation of VOCs including isoprene by OH produces an organic peroxy radical that converts nitric oxide (NO) to nitrogen dioxide (NO_2).[9] An organic oxy radical reacts with oxygen to form hydroperoxyl radical (HO_2), and the HO_2 additionally converts NO to NO_2.[9] In the presence of sunlight, photolysis of NO_2 forms O_3, which means that both isoprene and total NO_x ($NO + NO_2$) levels partially control O_3 production. Formaldehyde (HCHO) and other oxygenated VOCs are formed in the oxidation process. Furthermore, biogenic isoprene and monoterpenes are responsible for 60% of organic aerosol (OA), a major component of $PM_{2.5}$, over the southeastern US.[10] Isoprene and its intermediates participate in an elaborate

series of chemical reactions to form lower volatility products that partition into OA depending on the ambient conditions.[11] For example, isoprene species react with OH and HO_2 to form isoprene epoxydiols (IEPOX) under low-NO_x conditions.[12] It is estimated that IEPOX, organonitrates, and tetrafunctional compounds each contribute to one-third of global isoprene secondary organic aerosol (SOA).[8] Yet, past studies have indicated many unknowns in isoprene chemistry, particularly the fate of isoprene nitrates.[13–15]

In atmospheric chemistry modeling, we need innovative ways for representing complex, nonlinear, multiphase, and multiscale chemical processes. Currently, the master chemical mechanism (MCM version 3.3.1) for isoprene oxidation involves 602 species and 1926 reactions, derived from theoretical studies and chamber experiments.[16] Adding 86 species and 358 reactions to a detailed, comprehensive mechanism of isoprene and terpene chemistry (MOZART) was shown to decrease the daily maximum surface O_3 bias of the CESM/CAM-chem model generally by 3-4 ppb in the eastern US, relative to the previous, smaller MOZART mechanism.[15] However, it is not always practical to capture the detailed chemistry in large-scale atmospheric chemical transport models (CTMs) including GEOS-Chem or chemistry-climate models (CCMs) due to excessive computational costs. Consequently, CTMs and CCMs often use reduced mechanisms while striving for accuracy within acceptable ranges as a trade-off. Even in reduced form, chemistry involving isoprene is one of the most computationally-intensive components in these models.

To date, chemical mechanism reduction has been mostly performed manually by expert air quality scientists and software developers through techniques such as chemical lumping and empirical parameterization. Condensing the mechanism may occur in several stages including isomer grouping, applying steady-state approximation, and lumping minor and latter pathways together.[17] Species are also lumped, resulting in different nomenclature across mechanisms employed in CTMs.[8] The reduced mechanisms typically lack flexibility to adapt to new environmental conditions and require significant labor, time, and resources to make further updates. Updates are infrequent and susceptible to errors. Therefore, automating the reduction of chemical mechanisms to speed up the integration of chemical kinetics is an attractive, viable alternative.[18,19] Recently, we used a directed-graph path-based automated model reduction (AMORE) approach to develop a novel reduced isoprene oxidation mechanism (version 1.0) which outperformed other common mechanisms in the Framework for 0-D Atmospheric Modeling (F0AM) and Community Multiscale Air Quality (CMAQ) models.[19] A few studies have applied graph theory in reducing mechanisms in atmospheric chemistry, although it is has not widely been used.[19–21]

Here, we incorporate an updated AMORE isoprene oxidation mechanism (version 1.1) into the Kinetic PreProcessor (KPP), the chemistry-solver of the GEOS-Chem chemical transport model. We describe the configuration of year-long global and nested-grid eastern US (EUS) simulations. Both ground-based (AQS/IMPROVE) and satellite observations (TROPOMI/CrIS) were used to evaluate the GEOS-Chem model with the AMORE mechanism. We primarily aim to understand the effects of AMORE on GEOS-Chem (1) computational efficiency and (2) accuracy in predictions of air pollutants and related chemical species ($PM_{2.5}$, O_3, NO_2, HCHO, and total organic carbon). Finally, we examine the sensitivities of summertime air pollutant levels to biogenic isoprene and anthropogenic emissions across the EUS.

2. Methods

2.1. AMORE Isoprene Oxidation Mechanism

The new reduced gas-phase isoprene oxidation mechanism was developed using the AMORE algorithm.[19] This algorithm takes a large, high-fidelity input mechanism, such as the "Caltech full mechanism" based on Wennberg et al. (2018)[17] which was expanded in Wiser et al. (2023),[19] and reduces it to a much smaller size for 3D atmospheric models where time savings are critical. A set of priority species are given for the reduced mechanism to include. For the AMORE mechanism, these species were isoprene, isoprene epoxydiols (lumped), isoprene nitrates (lumped), glyoxal, methylglyoxal, methacrolein, methyl vinyl ketone, peroxyacetyl nitrate, methyl radical, and peroxyacetyl radical. The algorithm uses the graph representation of the full mechanism, in which species are nodes and reactions consist of sets of edges, as a starting point for analysis and reduction. Baseline and elevated concentrations were given as inputs for reactive species that were not structurally related to the compound being modeled: OH (1×10^{-6} ppb, 1×10^{-4} ppb), HO_2 (0.04 ppb, 0.2 ppb), NO (1.17×10^{-6} ppb, 0.53 ppb), NO_2 (1×10^{-4} ppb, 0.01 ppb), NO_3 (2.3×10^{-4} ppb, 0.02 ppb), O_3 (16.7 ppb, 100 ppb), and methyl peroxy radical (0.1 ppb, 0.2 ppb). In addition, baseline and elevated photolysis rate scale factors (0, 1) were provided. With a constant temperature of 292 K and pressure of 1000 hPa, the algorithm rapidly estimated the yields of all priority species for every possible combination of high and low values for the reactive species and photolysis.

Sequences of reactive species (and photolysis) were then assessed for their relative importance in determining the yields of the priority species, based on how much the yield of

priority species changed when any one of the reactive species was removed from the sequence. The most important sequences of reactive species (and photolysis) were those which most significantly changed the yields of priority species. A set of the most important sequences was used to create a new reduced mechanism, in which sequences of reactive species or photolysis form sequences of reactions involving the modeled compound (in this case isoprene) as the starting species, reacting with each reactive species in the sequence to form further oxidized intermediates, and finally ending the production of the priority species. By including multiple important sequences, a reduced mechanism with a small number of intermediates and total reactions was formed. The priority species' stoichiometric coefficient terms were determined by the yield of the priority species under conditions in which the given sequence was favored. All rate constants were assigned based on representative rate parameters for the reaction type. Since nitrogen oxides and oxidants were included in the AMORE algorithm as reactants but not as products, manual adjustments of their presence were made to increase the accuracy of the original AMORE mechanism. For a detailed description of the development of this AMORE version 1.0 isoprene oxidation mechanism, see Wiser et al. (2023).[19]

Minor updates were made to the version 1.0 mechanism based on initial GEOS-Chem testing. Most of the isoprene species were renamed to match existing, similar nomenclature accepted in GEOS-Chem. As excessive O_3 produced from NO_2 in the AMORE version 1.0 mechanism was observed, we opted to remove one artifact, NO_2 produced in the isoprene peroxide (IDCHP) + OH reaction, which lowered O_3 to near the baseline levels. Displayed in Tables 1 and 2, the AMORE isoprene version 1.1 mechanism comprises 12 species and 23 reactions. The default GEOS-Chem isoprene oxidation mechanism (mini Caltech) is described in Bates and Jacob (2019)[8] and will be referred to as BASE. Compared to BASE, AMORE is smaller by 43 species and 167 reactions. A copy of the BASE mechanism was replaced with our final AMORE version 1.1 mechanism in the Kinetic PreProcessor (KPP) version 2.3.3, the chemical solver of GEOS-Chem.[22] Including non-isoprene chemistry, the entire BASE mechanism in KPP consists of 291 species and 903 reactions. KPP takes a list of species, reactions, and rate constants as inputs, solves the chemical kinetics for the given mechanism, and outputs Fortran 90 code that gets compiled in GEOS-Chem.[18,23,24] We built compilable code in KPP with the BASE and AMORE mechanisms separately.

Table 1. A list of the 12 isoprene species participating in AMORE mechanism. Dummy species to track oxidation of isoprene by OH (LISOPOH) and NO_3 (LISOPNO3) are excluded.

#	Species Name	AMORE Nomenclature	GEOS-Chem Nomenclature
1	Isoprene	ISOP	ISOP
2	Isoprene nitrate	INO2	INO2B
3	Isoprene peroxy radical	IHOO	IHOO1
4	Isoprene peroxide	ISHP	IDCHP
5	Isoprene hydroxy nitrate	IHN	IHN1
6	Isoprene peroxy nitrate	IPN	INPB
7	Lumped higher order isoprene nitrates	ISON	IDN
8	Isoprene lumped peroxy carbonyl + other functional groups	IPC	IDC
9	Isoprene epoxydiol	IEPOX	IEPOXA
10	Isoprene-4,1-hydroxyaldehyde	HC5A	HC5A
11	Aerosol-phase organic nitrate from isoprene precursors	IONITA	IONITA
12	Aerosol-phase IEPOX	SOAIE	SOAIE

Table 2. The AMORE isoprene oxidation mechanism (23 reactions) as integrated into KPP. Heterogeneous reactions are not counted. Photolysis of IDCHP is calculated externally by the default FAST-JX version 7.0a photolysis mechanism. T is temperature (K).

#	Reaction	Rate Constant
1	ISOP + O3 → 0.189 MVK + 0.58 CH2O + 0.25 OH + 0.25 HO2 + 0.08 MO2 + 0.1 MCO3 + 0.09 H2O2 + 0.461 MACR + 0.14 CO	$1.58 \times 10^{-14} \exp(-2000/T)$ cm^3 mol^{-1} s^{-1}
2	ISOP + NO3 → INO2B + 0.3 CH2O + 0.3 NO2 + 0.3 IDN + LISOPNO3	$2.95 \times 10^{-12} \exp(-450/T)$ cm^3 mol^{-1} s^{-1}
3	ISOP + OH → IHOO1 + 0.02 MO2 + LISOPOH	$2.69 \times 10^{-11} \exp(390/T)$ cm^3 mol^{-1} s^{-1}
4	IHOO1 + HO2 → IDCHP + 0.6 HO2 + 0.15 CH2O	$4.5 \times 10^{-13} \exp(1300/T)$ cm^3 mol^{-1} s^{-1}
5	IHOO1 + NO → 0.14 IHN1 + 0.7 CH2O + 0.44 MVK + 0.88 HO2 + 0.78 NO2 + 0.28 MACR + 0.021 GLYX	$2.7 \times 10^{-12} \exp(350/T)$ cm^3 mol^{-1} s^{-1}
6	IDCHP + OH → IHOO1	$4.6 \times 10^{-12} \exp(200/T)$ cm^3 mol^{-1} s^{-1}
7	INO2B + HO2 → INPB + OH	$3.14 \times 10^{-14} \exp(580/T)$ cm^3 mol^{-1} s^{-1}
8	INO2B + NO → 0.9 CH2O + 0.5 MGLY + 0.8 MVK + 0.5 NO2 + HO2 + 0.2 IDN + 0.1 MO2	$9.42 \times 10^{-16} \exp(580/T)$ cm^3 mol^{-1} s^{-1}
9	INPB + HO2 → 0.8 NO2 + 0.4 CH2O + 0.05 GLYX + 0.1 MGLY + 0.4 MACR + HO2 + 0.94 MVK + 0.2 IDN + 0.1 MO2	$3.4 \times 10^{-11} \exp(390/T)$ cm^3 mol^{-1} s^{-1}
10	IHN1 + OH → IDN + OH + 0.2 IEPOXA	$2.4 \times 10^{-7} \exp(580/T)$ cm^3 mol^{-1} s^{-1}
11	IDCHP + OH → 0.15 CH2O + 0.05 MGLY + 0.15 MACR + 0.02 GLYX + 0.2 MVK + 0.05 IDC + 0.58 IEPOXA + 0.8 OH	$2.97 \times 10^{-11} \exp(390/T)$ cm^3 mol^{-1} s^{-1}
12	IDC + NO → 0.35 NO2 + 0.8 NO	1×10^{-10} cm^3 mol^{-1} s^{-1}
13	IDN + OH → CO + 0.12 NO2	5×10^{-11} cm^3 mol^{-1} s^{-1}
14	IDN + NO3 → CO	2×10^{-14} cm^3 mol^{-1} s^{-1}
15	IEPOXA + OH → OH	$5 \times 10^{-11} \exp(-400/T)$ cm^3 mol^{-1} s^{-1}
16	IHN1 → HNO3	2.3×10^{-5} cm^3 mol^{-1} s^{-1}
17	IHOO1 + MCO3 → 0.5 HO2 + 0.5 MO2 + 1.048 CH2O + 0.219 MACR + 0.305 MVK	$8.4 \times 10^{-14} \exp(221/T)$ cm^3 mol^{-1} s^{-1}
18	IHOO1 + IHOO1 → 2 MVK + 2 HO2 + 2 CH2O	6.92×10^{-14} $[1.1644 + (-7.0485 \times 10^{-4}) T]$ cm^3 mol^{-1} s^{-1}
19	IHOO1 + MO2 → MVK + 2 HO2 + 2 CH2O	2×10^{-12} $[1.1644 + (-7.0485 \times 10^{-4}) T]$ cm^3 mol^{-1} s^{-1}
20	IHOO1 + MO2 → CH2O + 0.5 HC5A + 1.5 HO2 + 0.5 MVKHP + 0.5 CO + 0.5 OH	2×10^{-12} $[-0.1644 + (7.0485 \times 10^{-4}) T]$ cm^3 mol^{-1} s^{-1}
21	HC5A + OH → 1.065 OH + 0.355 CO2 + 0.638 CO + 0.355 MGLY + 0.283 HO2 + 0.125 MVKHP + 0.158 MCRHP	$4.64 \times 10^{-12} \exp(650/T)$ cm^3 mol^{-1} s^{-1}
22	Cl + ISOP → HCl + IHOO1	$7.6 \times 10^{-11} \exp(500/T)$ cm^3 mol^{-1} s^{-1}
23	IDCHP + hv → 0.4 CH2O + 0.1 MGLY + 0.06 MCO3	PHOTOL(IDCHP)

2.2. GEOS-Chem Model Simulations

GEOS-Chem is a global 3D Eulerian CTM accessed freely and used by research groups worldwide to investigate atmospheric chemistry (http://geos-chem.org, last access: 1 August 2023). We set up the GEOS-Chem "Classic" version 13.3.3 model[25] on Columbia's "Ginsburg" High Performance Computing Cluster to conduct all simulations on a single node with two Intel Xeon Gold 6226 2.9 GHz central processing units, 32 cores, and 192 GB (for coarser-resolution simulations) or 768 GB (for higher-resolution simulations) of memory. All simulations were configured with full chemistry, complex SOA, and semi-volatile primary organic aerosol (POA) for 2018–2019. We designated the first five months as the model spin-up period and the period June 2018 – May 2019 for our analysis. Complex SOA and semi-volatile POA were selected over simple SOA and non-volatile POA because the former combination relies on a more sophisticated volatility basis set approach that improves correlation with observations.[11,26,27] Output diagnostic files included monthly-averaged aerosol mass concentrations, species concentrations, and reaction rates as well as daily boundary conditions. Timers in GEOS-Chem were enabled for the BASE and AMORE isoprene mechanism simulations to compare total run (wall-clock) times and estimate computational speed gained by running AMORE over BASE. As presented in Table 3, we performed 10 out of the 12 simulations globally at 2° × 2.5° horizontal resolution. These simulations were configured with all 72 hybrid sigma vertical levels; 10-minute timesteps for transport, cloud convection, planetary boundary layer (PBL) mixing, and wet deposition; and 20-minute timesteps for chemistry, emissions, and dry deposition. To optimize computational efficiency and simulation accuracy, chemical operator duration is recommended to be twice the transport operator duration.[28] We used Modern-Era Retrospective analysis for Research and Applications, version 2 (MERRA-2) meteorological products to drive the coarser-resolution simulations.

Using boundary conditions from the BASE 2° × 2.5° run, we also performed two 0.25° × 0.3125° nested-grid simulations (BASE_HR and AMORE_HR), over the eastern half of the US: latitude = [24°, 49°] and longitude = [-100°, -66°]. Tracer concentrations are known to be unrealistic on the edges of the nested grid domain where there is no advection.[29] Therefore, we applied a buffer zone of 3° along each of the four boundaries. The goal was to focus on peak summertime isoprene emissions over the southeastern US, but we expanded this domain to include the more forested, humid, and densely-populated urban areas east of the 100th meridian. Particularly in the northeastern US, anthropogenic emissions interact with biogenic emissions to form ground-level O_3 in the summertime.[30] The higher-resolution model had 47

vertical levels, extending from the surface to 0.01 hPa as in the 72-layer model, but with a coarser resolution to save computational resources. Transport, cloud convection, PBL mixing, and wet deposition cycled on 5-minute time steps, while chemistry, emissions, and dry deposition cycled on 10-minute time steps. Instead of MERRA-2, Goddard Earth Observing System-forward processing (GEOS-FP) meteorology was used for the higher-resolution simulations. MERRA-2 and GEOS-FP are similar and both originate from the NASA Global Modeling and Assimilation Office, though GEOS-FP offers the finer native horizontal resolution (0.25° × 0.3125°) that is not available with MERRA-2.

To quantify contributions from biogenic isoprene and anthropogenic emissions to air pollution levels in our EUS domain via both isoprene mechanisms, we perturbed emissions in eight sensitivity simulations (Table 3). Emissions are processed by the Harvard–NASA Emissions Component (HEMCO) module.[31] First, we defined a scale factor to zero out emissions over the contiguous US: latitude = [20°, 60°] and longitude [-140°, -50°]. Thereafter, we applied this scale factor to isoprene from the Model of Emissions of Gases and Aerosols from Nature (MEGAN) version 2.1 for the zUS_ISOP simulations.[5] Total biogenic isoprene emissions over the EUS domain in the coarser-resolution simulations (12.16 Tg C yr^{-1}) and higher-resolution (12.55 Tg C yr^{-1}) simulations are comparable. For the zUS_ANTH simulations, the same scale factor was applied to the following anthropogenic emissions sources: the Community Emissions Data System version 2,[32] ethane,[33] propane,[34] the Aviation Emissions Inventory Code,[35] ship emissions,[32] and anthropogenic fugitive, combustion, and industrial dust.[36] These anthropogenic emissions include sulfur dioxide (SO_2), carbon monoxide (CO), NO_x, PM, and VOCs. Soil NO_x emissions including fertilizer NO_x are left on and are similar in the coarser-resolution simulations (0.23 Tg N yr^{-1}) and higher-resolution simulations (0.22 Tg N yr^{-1}). Combining the aforementioned methods, both biogenic isoprene and anthropogenic emissions were zeroed out for the zUS_ISOP_ANTH simulations. Finally, we turned off the same anthropogenic emissions inventories globally for the zGLB_ANTH simulations.

Table 3. All 12 GEOS-Chem sensitivity simulations conducted in this study.

#	Simulation Name	Isoprene Chemistry	Emissions Perturbation	Horizontal Resolution
1	BASE	Default	None	2° × 2.5°
2	AMORE	AMORE	None	2° × 2.5°
3	BASE_HR	Default	None	0.25° × 0.3125°
4	AMORE_HR	AMORE	None	0.25° × 0.3125°
5	BASE_zUS_ISOP	Default	US biogenic isoprene set to zero	2° × 2.5°
6	AMORE_zUS_ISOP	AMORE	US biogenic isoprene set to zero	2° × 2.5°
7	BASE_zUS_ANTH	Default	US anthropogenic set to zero	2° × 2.5°
8	AMORE_zUS_ANTH	AMORE	US anthropogenic set to zero	2° × 2.5°
9	BASE_zUS_ISOP_ANTH	Default	US biogenic isoprene and anthropogenic set to zero	2° × 2.5°
10	AMORE_zUS_ISOP_ANTH	AMORE	US biogenic isoprene and anthropogenic set to zero	2° × 2.5°
11	BASE_zGLB_ANTH	Default	Global anthropogenic set to zero	2° × 2.5°
12	AMORE_zGLB_ANTH	AMORE	Global anthropogenic set to zero	2° × 2.5°

2.3. Evaluating Model Against Observations

Table 4 provides an overview of the observed data used to evaluate the model: (1) surface $PM_{2.5}$ and O_3 from the US EPA's Air Quality System (AQS) network, (2) surface total organic carbon (OC) from the Interagency Monitoring of Protected Visual Environments (IMPROVE) network, (3) NO_2 and HCHO tropospheric vertical column densities (VCDs) from the Tropospheric Monitoring Instrument (TROPOMI), and (4) isoprene total VCD from the Cross-track Infrared Sounder (CrIS). We obtained AQS/IMPROVE data for June 2018 – May 2019, removed any negative daily average concentrations, and selected days without any gaps in hourly measurements. For each AQS/IMPROVE variable, the concentrations were averaged by month. While the AQS/IMPROVE sites provide valuable in-situ point measurements with high temporal coverage, they are unevenly distributed and have less spatial coverage compared to satellite remote sensing data which measure total atmospheric columns and not only the

surface layer. In particular, AQS instruments are sensitive to local, urban pollution that tend to not be representative of entire model grid boxes for short-lived species including NO_2, HCHO, and isoprene.

The European Space Agency's Sentinel-5 Precursor (S5P) is a sun-synchronous, polar-orbiting satellite with a daily equator overpass time of 13:30 local time.[37] TROPOMI is a nadir-viewing spectrometer aboard the S5P, measuring NO_2 and HCHO columns in the ultraviolet-visible-near-infrared spectral bands at 3.5 km × 7 km resolution. In addition to higher spatial resolution, TROPOMI has a better signal-to-noise ratio compared with its predecessor, the Ozone Monitoring Instrument (OMI), but still exhibits regional biases including overestimating small HCHO columns and underestimating high HCHO columns.[38] We re-gridded TROPOMI Level 2 quality-controlled retrievals, transitioning from reprocessed (RPRO) and offline (OFFL) products on 28 November 2018, to 0.05° × 0.05° daily from June 2018 – May 2019. As recommended,[39,40] we selected pixels with quality assurance (QA) values greater than 0.75 for NO_2 and QA > 0.5 for HCHO, removing errors and observations influenced by cloud, snow, or ice cover. TROPOMI NO_2 and HCHO tropospheric VCDs, averaging kernels, and vertical pressure levels were averaged monthly.

CrIS is a Fourier transform spectrometer aboard the US National Oceanic and Atmospheric Administration's Suomi-NPP and NOAA-20 sun-synchronous satellites which have daily overpass times of about 13:30 and 12:40 local time.[41] We use the Retrieval of Organics from CrIS Radiances (ROCR) isoprene retrievals[42] at 0.5° × 0.625° resolution from Wells et al. (2022)[41] who employ a feed-forward neural network to derive total isoprene columns from CrIS hyperspectral range indices. Averaging kernels or other satellite observation operators are not available through this machine learning framework, and the products are averaged each month of year over the period 2012-2020. As a result, GEOS-Chem and CrIS should be compared more qualitatively.

To evaluate GEOS-Chem against TROPOMI and CrIS, we first converted NO_2, HCHO, and isoprene mole fractions for each 3D grid box from all GEOS-Chem simulations to partial tropospheric (NO_2 and HCHO) or total (isoprene) columns. The calculation required air temperature, specific humidity, surface pressure, and tropopause pressure from both the MERRA-2 and GEOS-FP meteorological products for the coarser and higher-resolution simulations, respectively. For consistency between modeled and observed vertical profiles, we applied TROPOMI averaging kernels at TROPOMI vertical pressure levels nearest to GEOS-Chem vertical pressure levels. This was performed by multiplying partial tropospheric columns (re-gridded to 0.05° x 0.05°) by averaging kernels on the same grid and then integrating from

the surface up to the nonuniform tropopause. Isoprene partial columns were simply integrated from the surface to the top of the atmosphere. For all variables listed in Table 4, we selected observations within latitude = [27°, 46°] and longitude = [-97°, -69°] to exclude the buffer zone of the nested-grid simulations. The nearest model grid box to each AQS/IMPROVE site or TROPOMI/CrIS grid box was found, differences between the monthly predicted and observed values were calculated, and these differences were averaged by season and over the year.

Table 4. Summary of observed data processed from AQS/IMPROVE monitoring sites (FRM/FEM for $PM_{2.5}$) and TROPOMI/CrIS satellite retrievals.

Variable	Units	Number of Sites / Spatial Resolution	Data Source
Surface $PM_{2.5}$	μg m^{-3}	606 sites	US Environmental Protection Agency AirData[43]
Surface O_3	ppb	765 sites	US Environmental Protection Agency AirData[43]
Surface total OC	μg m^{-3}	43 sites	Colorado State University Federal Land Manager Environmental Database[44]
NO_2 tropospheric VCD	molecules cm^{-2}	0.05° × 0.05°	NASA Goddard Earth Sciences Data and Information Services Center[45]
HCHO tropospheric VCD	molecules cm^{-2}	0.05° × 0.05°	NASA Goddard Earth Sciences Data and Information Services Center[46]
Isoprene total VCD	molecules cm^{-2}	0.5° × 0.625°	University of Minnesota Data Repository[42]

3. Results and Discussion

3.1. Computational Efficiency

Table 5 summarizes the speed of BASE versus AMORE GEOS-Chem simulations through total wall-clock times. AMORE was faster than BASE by about 19 hours for the entire year simulated at 2° × 2.5° resolution. This speedup was about 10% in total and 25% in the gas- and aqueous-phase chemical reaction solver (KPP), the latter within the expected range of 20-32% reported by Lin et al. (2023)[18] who used an adaptive solver option to reduce comprehensive oxidant-aerosol chemistry. At 0.25° × 0.3125° resolution, AMORE was again faster than BASE, by about 2% in total and 20% in KPP. In general, the higher-resolution simulations took approximately three times longer than the coarser-resolution simulations, within the range described in Philip et al. (2016).[28] Finer external time steps and boundary conditions partly contribute to longer wall-clock times at higher resolutions.[18,28] Only the rates of the first two reactions in both chemical mechanisms were saved as diagnostic output by default in the higher-resolution simulations, whereas additional rates in the BASE (38 reactions) and AMORE (25 reactions) isoprene oxidation mechanisms were saved in the coarse-resolution simulations. The difference in diagnostic output between mechanisms mostly explains the greater total GEOS-Chem speedup at 2° × 2.5° resolution. Our results demonstrate that reducing the isoprene oxidation mechanism alone can significantly expedite the model. Even with the same model configurations, wall-clock times may vary depending on other processes on the system and across different high-performance computing systems. Repeated model simulations would increase the confidence in the wall-clock times presented here.

Table 5. GEOS-Chem timer statistics comparing BASE and AMORE. Total wall-clock times are sums of monthly simulation times from June 2018 – May 2019, reported for both the coarser and higher-resolution simulations.

Timer Name	Horizontal Resolution	BASE (hours)	AMORE (hours)	AMORE - BASE Difference (hours)	AMORE - BASE Change (%)
GEOS-Chem	2° × 2.5°	181.2	162.6	-18.5	-10.2
KPP	2° × 2.5°	44.0	33.1	-10.8	-24.6
GEOS-Chem	0.25° × 0.3125°	496.3	485.9	-10.4	-2.1
KPP	0.25° × 0.3125°	44.9	35.8	-9.1	-20.3

3.2. Air Pollutants and Related Chemical Species

In Figure 1, model performance statistics compare BASE, AMORE, BASE_HR, and AMORE_HR against observational data averaged over June 2018 – May 2019 across the EUS. Overall, there are minor differences between BASE and AMORE as well as between BASE_HR and AMORE_HR. Two-sample *t*-tests show that, over the entire EUS model domain, there is not a statistically significant difference (*p*-value > 0.05) between BASE and AMORE for $PM_{2.5}$, NO_2, and total OC as well as between BASE_HR and AMORE_HR for $PM_{2.5}$ and NO_2. All simulations have low to moderate correlation ($0.25 < r < 0.51$) with observed annual mean $PM_{2.5}$, O_3, and total OC and high correlation ($0.82 < r < 0.89$) for NO_2 and HCHO. Resolution is particularly important for $PM_{2.5}$, O_3, and total OC, considering the correlation coefficient (r) increases by over 0.1 from the coarser to higher-resolution simulations, greater than differences related to the isoprene mechanism. Furthermore, normalized mean bias (NMB) for all variables except $PM_{2.5}$ is closer to zero for the higher-resolution simulations. The $PM_{2.5}$ negative bias and total OC (or OA) positive bias have been documented before, revealing uncertainties in biogenic isoprene and other aerosol species.[10,11] In addition, previous studies have indicated that GEOS-Chem overestimates O_3, in part due to excessive NO_x emissions.[47] The O_3 and HCHO positive biases are lower in both AMORE and AMORE_HR, although improvements elsewhere in the model are still needed to significantly reduce these biases. Likewise, AMORE_HR is less biased than BASE_HR in simulating total OC.

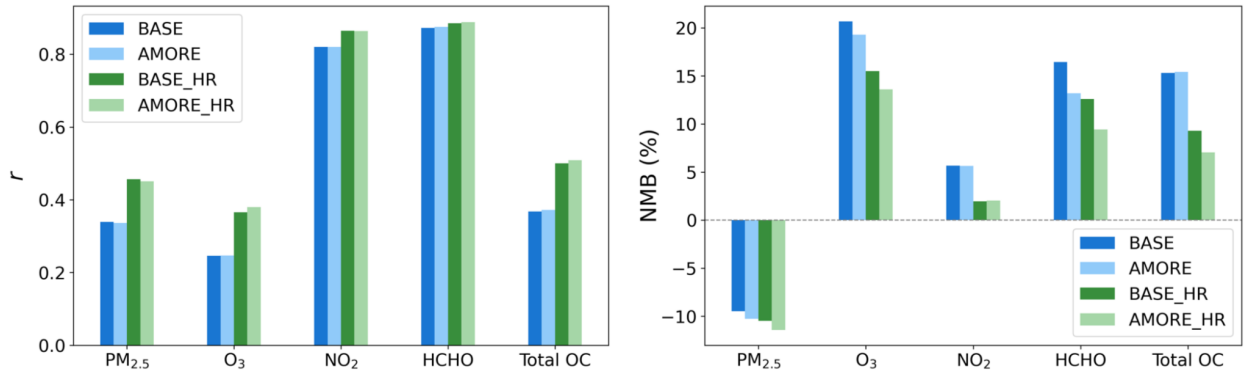

Figure 1. GEOS-Chem model performance statistics for annual (June 2018 – May 2019) mean $PM_{2.5}$, O_3, and NO_2 at AQS/IMPROVE sites and NO_2 and HCHO tropospheric VCDs at TROPOMI grid boxes across the EUS domain. Pearson's correlation coefficient (r) is on the left, and normalized mean bias (NMB) is on the right. For each of the five variables, the 2° × 2.5° (BASE and AMORE) and 0.25° × 0.3125° (BASE_HR and AMORE_HR) simulations were evaluated against observations.

Spatial distributions of the nested-grid EUS simulations compared with each other and against observations are presented in Figures 2 and 3. On average over the entire time period, $PM_{2.5}$ is lower by 0.11 μg m^{-3} (2.0%), O_3 is lower by 0.71 ppb (2.1%), total OC is lower by 0.04 μg m^{-3} (2.7%), NO_2 is higher by 0.02 ppb (1.7%), and HCHO is lower by 0.18 ppb (9.0%) in AMORE_HR relative to BASE_HR. Figure 2 shows that $PM_{2.5}$ is highest in states around the Great Lakes, influenced by anthropogenic emissions (Figure 2). Both simulations underpredict $PM_{2.5}$ on average, with the mean model bias just 0.07 μg m^{-3} (1%) lower in AMORE_HR than BASE_HR. O_3 is elevated along the coastline in the model and local areas such as within the southern Appalachians in the observations. A shallow marine PBL and topography, among other factors, can trap O_3. Both simulations overpredict O_3 on average, but AMORE_HR improves the mean model bias by 0.57 ppb (1%). Total OC (OA:OC = 2.1) is highest in the southeastern US, and AMORE_HR improves the mean model bias by 0.03 μg m^{-3} (2%).

Compared against TROPOMI, both BASE_HR and AMORE_HR slightly overpredict NO_2 on average to about the same degree, with the exception of several NO_2 hotspots in urban areas that the model underpredicts (Figure 3). Across the southeastern US, where HCHO and isoprene are enhanced in the domain, both simulations overpredict HCHO, but AMORE_HR improves the EUS mean model bias by 0.18 molecules cm^{-2} (4%). Relative to CrIS, both simulations largely underpredict isoprene across the EUS domain, possibly because of insufficient isoprene emissions and uncertainties in the satellite retrievals.[41] Isoprene is higher by 36.6% in AMORE_HR than BASE_HR which improves the mean model bias by 0.27 molecules cm^{-2} (18%). Higher isoprene domain-wide is beneficial, including for the “isoprene volcano” or Missouri Ozarks region which features a high density of strongly isoprene-emitting oak trees.[48] However, AMORE_HR does not improve the model bias for two prominent isoprene peaks to the south of the Missouri Ozarks.

Higher isoprene in AMORE_HR than BASE_HR suggests that less of it is oxidized in the AMORE mechanism. The main oxidant, OH, exhibits widespread lower concentrations with the AMORE mechanism than BASE mechanism. In low-NO_x conditions, reactions between isoprene peroxy radicals (IHOO1) and HO_2 tend to consume OH which can be regenerated through more intramolecular hydrogen shifts.[8] Less OH recycling and thus lower OH concentrations are expected with fewer intermediate species in the AMORE mechanism, on par with other similarly sized reduced mechanisms.[19] Higher isoprene may also emphasize the low-NOx pathway, leading to further OH depletion and hindering NO_2 production. Reaction rates for ISOP + OH and ISOP + O_3 are the same order of magnitude but lower and higher in the AMORE mechanism, respectively. Since the rate constants are about the same in both mechanisms,

changes in species concentrations are likely responsible for the reaction rate differences. While the latter reaction depletes O_3 and is more competitive in the AMORE mechanism, ISOP + OH happens faster, and lower HCHO signifies the impact of less OH-initiated oxidation. A lower ISOP + NO_3 reaction rate in the AMORE mechanism than BASE mechanism, due to a rate constant discrepancy, could allow less NO_x to be lost to isoprene nitrates. We find that the ISOP + NO_3 rate constant matches that in Wennberg et al. (2018),[17] lower by 1-2 orders of magnitude than in the BASE mechanism. See Figure S1 in the supplementary information for global spatial differences in annual mean concentrations of $PM_{2.5}$, O_3, and other key chemical species between the BASE and AMORE simulations.

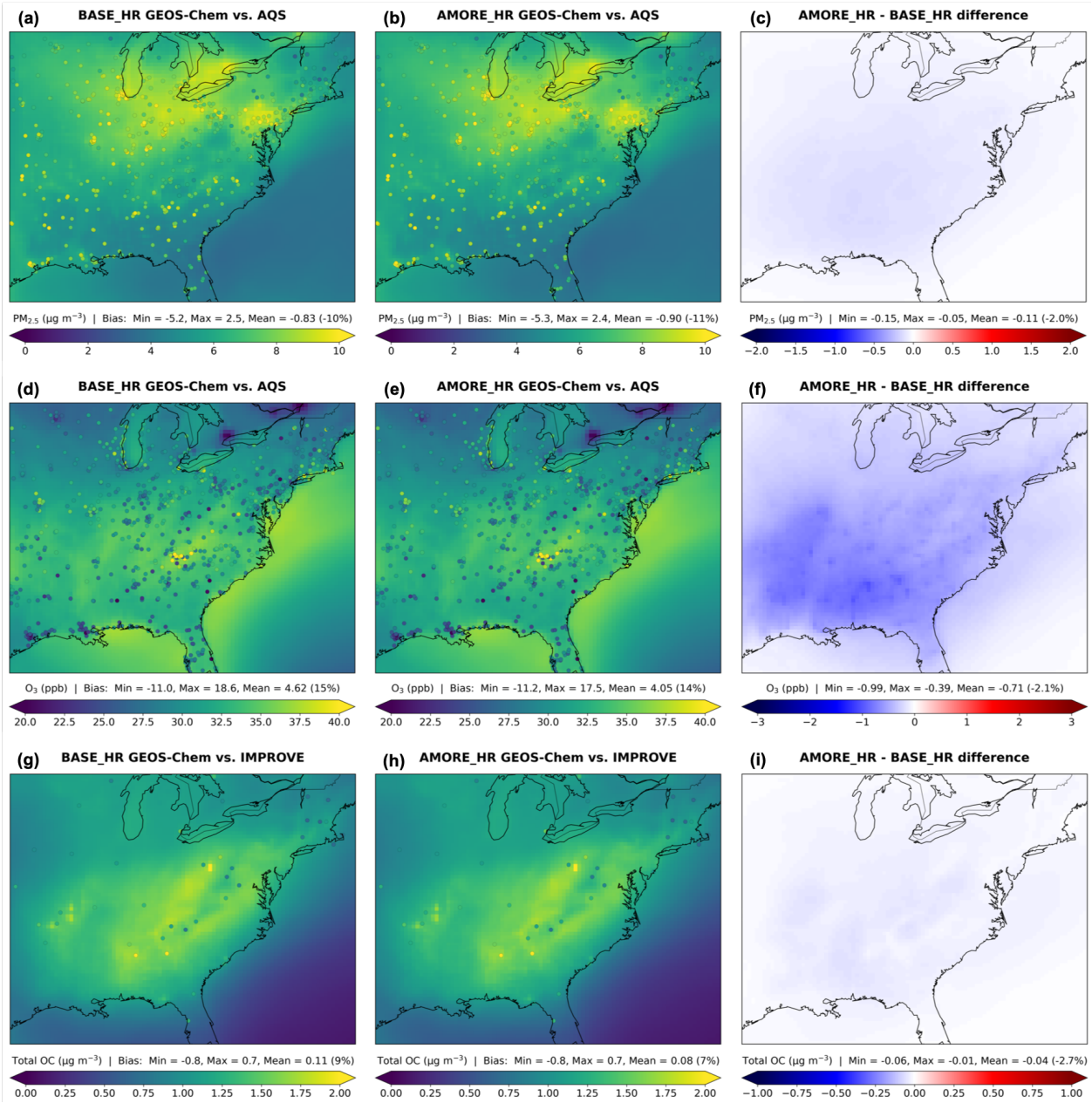

Figure 2. EUS maps of 0.25° × 0.3125° GEOS-Chem simulated annual (June 2018 – May 2019) mean (a-c) $PM_{2.5}$ (μg m^{-3}), (d-f) O_3 (ppb), and (g-i) total OC (μg m^{-3}). BASE_HR (left column) and AMORE_HR (center column) simulations are compared with AQS/IMPROVE observations (dots). Minimum, maximum, and mean model biases (modeled - observed) are calculated over EUS sites. Differences (right column) between the simulations represent lower (blue) or higher (red) concentrations in AMORE_HR than BASE_HR.

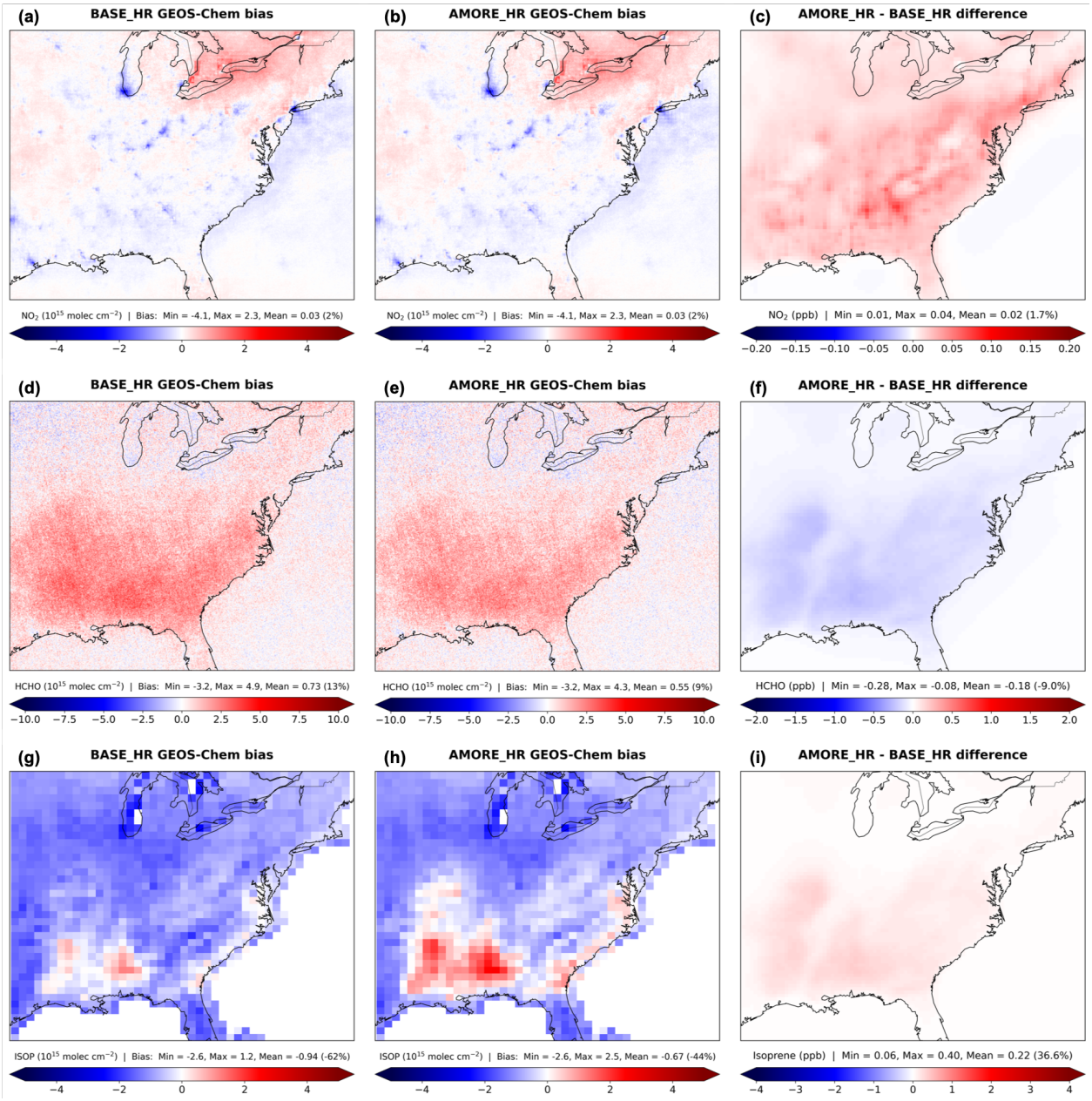

Figure 3. A comparison between the EUS 0.25° x 0.3125° GEOS-Chem simulations and TROPOMI/CrIS observations for annual (June 2018 – May 2019) mean (a-c) NO_2 tropospheric VCD, (d-f) HCHO tropospheric VCD, and (g-i) isoprene total VCD, all in units of 10^{15} molecules cm^{-2}. BASE_HR (left column) and AMORE_HR (center column) biases (modeled - observed) indicate either overprediction (red) or underprediction (blue). Differences (right column) between the simulations indicate that AMORE_HR is higher (red) or lower (blue) than BASE_HR.

3.3. Sensitivities of Air Pollutants to Biogenic Isoprene and Anthropogenic Emissions

Now, we focus our analysis on the summertime when isoprene emissions peak in the region of interest. For all seasons and sensitivity maps, see Figures S2 and S3 in the supplementary information. Figure 4 displays average EUS summer 2018 percent changes in concentration responses of $PM_{2.5}$, O_3, NO_2, HCHO, and total OC to biogenic and anthropogenic emissions in BASE and AMORE compared with the eight sensitivity simulations in which emissions were zeroed out. On average, we estimate that US biogenic isoprene emissions (blue box plots) contribute to 0.5-0.6 μg m^{-3} (7-9%) of $PM_{2.5}$ and 1.1-1.7 ppb (3-4%) of O_3. US anthropogenic emissions (green box plots) contribute to about 2.2 μg m^{-3} (32-34%) of $PM_{2.5}$ and 17.6-18.1 ppb (43-45%) of O_3. Together, US biogenic isoprene and anthropogenic emissions (green box plots) contribute to about 2.5-2.7 μg m^{-3} (38-40%) of $PM_{2.5}$ and 15.6-16.1 ppb (39%) of O_3. These changes are not equal to those from separate isoprene and anthropogenic emissions summed together because of nonlinearities in the model. Adding in isoprene emissions subtly decreases O_3 levels over some of the southeastern US, perhaps scavenging OH that would otherwise produce more O_3 through reactions with other VOCs such as monoterpenes or sesquiterpenes.[15,49] Subtracting zGLB_ANTH from zUS_ANTH, we estimate that non-US anthropogenic emissions (yellow box plots) contribute to 0.2 μg m^{-3} (4%) of $PM_{2.5}$ and 1.8-2.1 ppb (8-10%) of O_3.

Unlike $PM_{2.5}$ and O_3, HCHO and total OC are much more sensitive to isoprene, with increases of 49-54% (HCHO) and 50-51% (total OC) from US biogenic isoprene emissions alone and increases of 68-71% (HCHO) and 63-64% (total OC) from the combination of US isoprene and anthropogenic emissions. US anthropogenic emissions are responsible for the majority of NO_2 (84-85%) which decreases slightly when adding in biogenic isoprene emissions. For all air pollutants, little differences exist between the BASE and AMORE simulations, suggesting that we can use the computationally-efficient AMORE approach without sacrificing process-level understanding gained from the perturbation simulations.

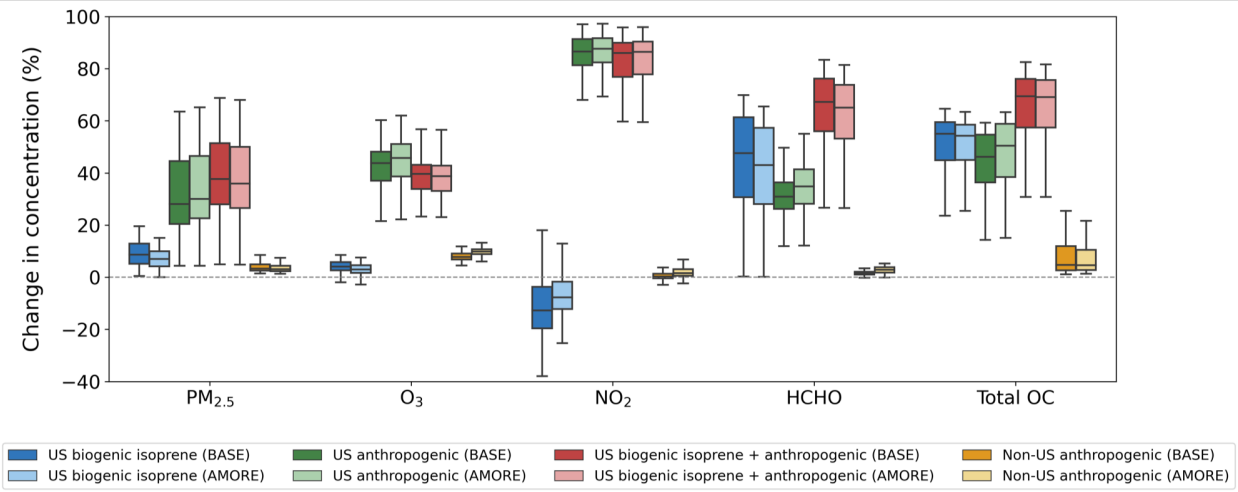

Figure 4. Summer average (June–August 2018) sensitivities of atmospheric constituents to "adding in" different emissions across the EUS domain at 2° × 2.5° resolution. Percent changes of BASE minus BASE zero emissions (dark blue, green, and red) or AMORE minus AMORE zero emissions (light blue, green, and red) are relative to BASE or AMORE. Non-US anthropogenic (yellow) represents zUS_ANTH minus zGLB_ANTH. Each box plot shows the standard interquartile range (IQR) from the 25th (Q1) to 75th (Q3) percentiles, with whiskers extending to Q1 - (1.5 × IQR) and Q3 + (1.5 × IQR).

4. Conclusions

We have compared the new reduced (AMORE version 1.1) and default (BASE) isoprene oxidation mechanisms and their impacts on air pollutants in the GEOS-Chem model, both at 2° × 2.5° resolution globally and 0.25° × 0.3125° resolution over the EUS. Our study demonstrates that using the AMORE isoprene oxidation mechanism in GEOS-Chem not only saves computational resources but also maintains about the same or even improves model accuracy, including for model sensitivities to precursor emissions, over the EUS. While chemistry is important for predicting $PM_{2.5}$ and O_3, our results suggest that increasing the model resolution improves the model performance more than changing the isoprene mechanism. Moreover, the relatively small changes in air pollutant concentrations due to isoprene support the need to continue to significantly reduce US anthropogenic emissions to improve air quality in the context of projected biogenic VOC increases in a warming climate.[4,13]

Future development of reduced chemical mechanisms can benefit from our automated graph theory-based approach. We tested the AMORE algorithm for gas-phase isoprene oxidation, but there are potential applications to aqueous-phase chemistry or other mechanisms. More work is needed to make AMORE fully automated and sufficiently flexible for use in a wide range of chemical mechanisms and atmospheric models. A limitation of this study was the amount and quality of observational data available to evaluate the GEOS-Chem model. This model evaluation would benefit from more in-situ and remote sensing measurements of chemical species important to isoprene oxidation, such as HCHO and OA, in different photochemical regimes across the globe. For example, the Tropospheric Emissions Monitoring of Pollution (TEMPO) instrument, launched in April 2023, will provide daytime hourly air pollution information across North America from a geostationary orbit.[50] We are interfacing with the GEOS-Chem modeling team to make AMORE an option for all users in the standardized GEOS-Chem code. Improvements in computational speed and accuracy of CTMs and CCMs will allow for efficient air quality and climate forecasting, research, and management.

Code and Data Availability

The AMORE version 1.1 isoprene oxidation mechanism used in the Kinetic PreProcessor is available online: https://github.com/benjaminyang93/amore_v1.1 (last access: 1 August 2023). Additional supplemental files including the AMORE algorithm code are uploaded: https://github.com/fcw2110/AMORE_supplementary_files (last access: 1 August 2023). The GEOS-Chem model is publicly available (http://geos-chem.org).[25]

Conflicts of Interest

There are no conflicts of interest to declare.

Acknowledgments

This work was funded by the US Environmental Protection Agency under grant number 840013. The authors would like to thank Kelvin H. Bates and Sidhant J. Pai, with whom we had helpful discussions.

References

1 R. Fuller, P. J. Landrigan, K. Balakrishnan, G. Bathan, S. Bose-O'Reilly, M. Brauer, J. Caravanos, T. Chiles, A. Cohen, L. Corra, M. Cropper, G. Ferraro, J. Hanna, D. Hanrahan, H. Hu, D. Hunter, G. Janata, R. Kupka, B. Lanphear, M. Lichtveld, K. Martin, A. Mustapha, E. Sanchez-Triana, K. Sandilya, L. Schaefli, J. Shaw, J. Seddon, W. Suk, M. M. Téllez-Rojo and C. Yan, Pollution and health: a progress update, *Lancet Planet. Health*, 2022, **6**, e535–e547.

2 T. Li, R. Hu, Z. Chen, Q. Li, S. Huang, Z. Zhu and L.-F. Zhou, Fine particulate matter ($PM_{2.5}$): The culprit for chronic lung diseases in China, *Chronic Dis. Transl. Med.*, 2018, **4**, 176–186.

3 A. M. Fiore, V. Naik and E. M. Leibensperger, Air Quality and Climate Connections, *J. Air Waste Manag. Assoc.*, 2015, **65**, 645–685.

4 A. H. Goldstein, C. D. Koven, C. L. Heald and I. Y. Fung, Biogenic carbon and anthropogenic pollutants combine to form a cooling haze over the southeastern United States, *Proc. Natl. Acad. Sci.*, 2009, **106**, 8835–8840.

5 A. B. Guenther, X. Jiang, C. L. Heald, T. Sakulyanontvittaya, T. Duhl, L. K. Emmons and X. Wang, The Model of Emissions of Gases and Aerosols from Nature version 2.1 (MEGAN2.1):

an extended and updated framework for modeling biogenic emissions, *Geosci. Model Dev.*, 2012, **5**, 1471–1492.

6 T. D. Sharkey, A. E. Wiberley and A. R. Donohue, Isoprene Emission from Plants: Why and How, *Ann. Bot.*, 2008, **101**, 5–18.

7 D. F. McGlynn, L. E. R. Barry, M. T. Lerdau, S. E. Pusede and G. Isaacman-VanWertz, Measurement report: Variability in the composition of biogenic volatile organic compounds in a Southeastern US forest and their role in atmospheric reactivity, *Atmospheric Chem. Phys.*, 2021, **21**, 15755–15770.

8 K. H. Bates and D. J. Jacob, A new model mechanism for atmospheric oxidation of isoprene: global effects on oxidants, nitrogen oxides, organic products, and secondary organic aerosol, *Atmospheric Chem. Phys.*, 2019, **19**, 9613–9640.

9 D. J. Jacob, *Introduction to Atmospheric Chemistry*, Princeton University Press, 1999.

10 P. S. Kim, D. J. Jacob, J. A. Fisher, K. Travis, K. Yu, L. Zhu, R. M. Yantosca, M. P. Sulprizio, J. L. Jimenez, P. Campuzano-Jost, K. D. Froyd, J. Liao, J. W. Hair, M. A. Fenn, C. F. Butler, N. L. Wagner, T. D. Gordon, A. Welti, P. O. Wennberg, J. D. Crounse, J. M. St. Clair, A. P. Teng, D. B. Millet, J. P. Schwarz, M. Z. Markovic and A. E. Perring, Sources, seasonality, and trends of southeast US aerosol: an integrated analysis of surface, aircraft, and satellite observations with the GEOS-Chem chemical transport model, *Atmospheric Chem. Phys.*, 2015, **15**, 10411–10433.

11 S. J. Pai, C. L. Heald, J. R. Pierce, S. C. Farina, E. A. Marais, J. L. Jimenez, P. Campuzano-Jost, B. A. Nault, A. M. Middlebrook, H. Coe, J. E. Shilling, R. Bahreini, J. H. Dingle and K. Vu, An evaluation of global organic aerosol schemes using airborne observations, *Atmospheric Chem. Phys.*, 2020, **20**, 2637–2665.

12 F. Paulot, J. D. Crounse, H. G. Kjaergaard, A. Kürten, J. M. St. Clair, J. H. Seinfeld and P. O. Wennberg, Unexpected Epoxide Formation in the Gas-Phase Photooxidation of Isoprene, *Science*, 2009, **325**, 730–733.

13 A. M. Fiore, L. W. Horowitz, D. W. Purves, H. Levy II, M. J. Evans, Y. Wang, Q. Li and R. M. Yantosca, Evaluating the contribution of changes in isoprene emissions to surface ozone trends over the eastern United States, *J. Geophys. Res. Atmospheres*, DOI:10.1029/2004JD005485.

14 D. J. Jacob and D. A. Winner, Effect of climate change on air quality, *Atmos. Environ.*, 2009, **43**, 51–63.

15 R. H. Schwantes, L. K. Emmons, J. J. Orlando, M. C. Barth, G. S. Tyndall, S. R. Hall, K. Ullmann, J. M. St. Clair, D. R. Blake, A. Wisthaler and T. P. V. Bui, Comprehensive isoprene

and terpene gas-phase chemistry improves simulated surface ozone in the southeastern US, *Atmospheric Chem. Phys.*, 2020, **20**, 3739–3776.

16 M. E. Jenkin, J. C. Young and A. R. Rickard, The MCM v3.3.1 degradation scheme for isoprene, *Atmospheric Chem. Phys.*, 2015, **15**, 11433–11459.

17 P. O. Wennberg, K. H. Bates, J. D. Crounse, L. G. Dodson, R. C. McVay, L. A. Mertens, T. B. Nguyen, E. Praske, R. H. Schwantes, M. D. Smarte, J. M. St Clair, A. P. Teng, X. Zhang and J. H. Seinfeld, Gas-Phase Reactions of Isoprene and Its Major Oxidation Products, *Chem. Rev.*, 2018, **118**, 3337–3390.

18 H. Lin, M. S. Long, R. Sander, A. Sandu, R. M. Yantosca, L. A. Estrada, L. Shen and D. J. Jacob, An Adaptive Auto-Reduction Solver for Speeding Up Integration of Chemical Kinetics in Atmospheric Chemistry Models: Implementation and Evaluation in the Kinetic Pre-Processor (KPP) Version 3.0.0, *J. Adv. Model. Earth Syst.*, 2023, **15**, e2022MS003293.

19 F. Wiser, B. K. Place, S. Sen, H. O. T. Pye, B. Yang, D. M. Westervelt, D. K. Henze, A. M. Fiore and V. F. McNeill, AMORE-Isoprene v1.0: a new reduced mechanism for gas-phase isoprene oxidation, *Geosci. Model Dev.*, 2023, **16**, 1801–1821.

20 Z. M. Nikolaou, J.-Y. Chen, Y. Proestos, J. Lelieveld and R. Sander, Accelerating simulations using REDCHEM_v0.0 for atmospheric chemistry mechanism reduction, *Geosci. Model Dev.*, 2018, **11**, 3391–3407.

21 S. J. Silva, S. M. Burrows, M. J. Evans and M. Halappanavar, A Graph Theoretical Intercomparison of Atmospheric Chemical Mechanisms, *Geophys. Res. Lett.*, 2021, **48**, e2020GL090481.

22 The International GEOS-Chem User Community, geoschem/KPP: KPP-for-GEOS-Chem 2.3.3_gc, *Zenodo*, DOI:10.5281/zenodo.5140218.

23 V. Damian, A. Sandu, M. Damian, F. Potra and G. R. Carmichael, The kinetic preprocessor KPP-a software environment for solving chemical kinetics, *Comput. Chem. Eng.*, 2002, **26**, 1567–1579.

24 A. Sandu and R. Sander, Technical note: Simulating chemical systems in Fortran90 and Matlab with the Kinetic PreProcessor KPP-2.1, *Atmospheric Chem. Phys.*, 2006, **6**, 187–195.

25 The International GEOS-Chem User Community, geoschem/GCClassic: GEOS-Chem 13.3.3, *Zenodo*, DOI:10.5281/zenodo.5748260.

26 E. A. Marais, D. J. Jacob, J. L. Jimenez, P. Campuzano-Jost, D. A. Day, W. Hu, J. Krechmer, L. Zhu, P. S. Kim, C. C. Miller, J. A. Fisher, K. Travis, K. Yu, T. F. Hanisco, G. M. Wolfe, H. L. Arkinson, H. O. T. Pye, K. D. Froyd, J. Liao and V. F. McNeill, Aqueous-phase mechanism for secondary organic aerosol formation from isoprene: application to the southeast United

States and co-benefit of SO_2 emission controls, *Atmospheric Chem. Phys.*, 2016, **16**, 1603–1618.

27 H. O. T. Pye, A. W. H. Chan, M. P. Barkley and J. H. Seinfeld, Global modeling of organic aerosol: the importance of reactive nitrogen (NO_x and NO_3), *Atmospheric Chem. Phys.*, 2010, **10**, 11261–11276.

28 S. Philip, R. V. Martin and C. A. Keller, Sensitivity of chemistry-transport model simulations to the duration of chemical and transport operators: a case study with GEOS-Chem v10-01, *Geosci. Model Dev.*, 2016, **9**, 1683–1695.

29 Y. X. Wang, M. B. McElroy, D. J. Jacob and R. M. Yantosca, A nested grid formulation for chemical transport over Asia: Applications to CO, *J. Geophys. Res. Atmospheres*, DOI:10.1029/2004JD005237.

30 M. Tao, A. M. Fiore, X. Jin, L. D. Schiferl, R. Commane, L. M. Judd, S. Janz, J. T. Sullivan, P. J. Miller, A. Karambelas, S. Davis, M. Tzortziou, L. Valin, A. Whitehill, K. Civerolo and Y. Tian, Investigating Changes in Ozone Formation Chemistry during Summertime Pollution Events over the Northeastern United States, *Environ. Sci. Technol.*, 2022, **56**, 15312–15327.

31 C. A. Keller, M. S. Long, R. M. Yantosca, A. M. Da Silva, S. Pawson and D. J. Jacob, HEMCO v1.0: a versatile, ESMF-compliant component for calculating emissions in atmospheric models, *Geosci. Model Dev.*, 2014, **7**, 1409–1417.

32 R. M. Hoesly, S. J. Smith, L. Feng, Z. Klimont, G. Janssens-Maenhout, T. Pitkanen, J. J. Seibert, L. Vu, R. J. Andres, R. M. Bolt, T. C. Bond, L. Dawidowski, N. Kholod, J. Kurokawa, M. Li, L. Liu, Z. Lu, M. C. P. Moura, P. R. O'Rourke and Q. Zhang, Historical (1750–2014) anthropogenic emissions of reactive gases and aerosols from the Community Emissions Data System (CEDS), *Geosci. Model Dev.*, 2018, **11**, 369–408.

33 Z. A. Tzompa-Sosa, E. Mahieu, B. Franco, C. A. Keller, A. J. Turner, D. Helmig, A. Fried, D. Richter, P. Weibring, J. Walega, T. I. Yacovitch, S. C. Herndon, D. R. Blake, F. Hase, J. W. Hannigan, S. Conway, K. Strong, M. Schneider and E. V. Fischer, Revisiting global fossil fuel and biofuel emissions of ethane, *J. Geophys. Res. Atmospheres*, 2017, **122**, 2493–2512.

34 Y. Xiao, J. A. Logan, D. J. Jacob, R. C. Hudman, R. Yantosca and D. R. Blake, Global budget of ethane and regional constraints on U.S. sources, *J. Geophys. Res. Atmospheres*, DOI:10.1029/2007JD009415.

35 M. E. J. Stettler, S. Eastham and S. R. H. Barrett, Air quality and public health impacts of UK airports. Part I: Emissions, *Atmos. Environ.*, 2011, **45**, 5415–5424.

36 S. Philip, R. V. Martin, G. Snider, C. L. Weagle, A. van Donkelaar, M. Brauer, D. K. Henze, Z. Klimont, C. Venkataraman, S. K. Guttikunda and Q. Zhang, Anthropogenic fugitive,

combustion and industrial dust is a significant, underrepresented fine particulate matter source in global atmospheric models, *Environ. Res. Lett.*, 2017, **12**, 044018.

37 D. L. Goldberg, M. Harkey, B. de Foy, L. Judd, J. Johnson, G. Yarwood and T. Holloway, Evaluating NO_x emissions and their effect on O_3 production in Texas using TROPOMI NO_2 and HCHO, *Atmospheric Chem. Phys.*, 2022, **22**, 10875–10900.

38 C. Vigouroux, B. Langerock, C. A. Bauer Aquino, T. Blumenstock, Z. Cheng, M. De Mazière, I. De Smedt, M. Grutter, J. W. Hannigan, N. Jones, R. Kivi, D. Loyola, E. Lutsch, E. Mahieu, M. Makarova, J.-M. Metzger, I. Morino, I. Murata, T. Nagahama, J. Notholt, I. Ortega, M. Palm, G. Pinardi, A. Röhling, D. Smale, W. Stremme, K. Strong, R. Sussmann, Y. Té, M. van Roozendael, P. Wang and H. Winkler, TROPOMI–Sentinel-5 Precursor formaldehyde validation using an extensive network of ground-based Fourier-transform infrared stations, *Atmospheric Meas. Tech.*, 2020, **13**, 3751–3767.

39 H. Eskes and K.-U. Eichmann, S5P Mission Performance Centre Nitrogen Dioxide [L2__NO2___] Readme, *Eur. Space Agency ESA*, DOI:10.5270/S5P-9bnp8q8.

40 I. De Smedt, F. Romahn and K.-U. Eichmann, S5P Mission Performance Centre Formaldehyde [L2__HCHO___] Readme, *Eur. Space Agency ESA*, DOI:10.5270/S5P-vg1i7t0.

41 K. C. Wells, D. B. Millet, V. H. Payne, C. Vigouroux, C. a. B. Aquino, M. De Mazière, J. A. de Gouw, M. Graus, T. Kurosu, C. Warneke and A. Wisthaler, Next-Generation Isoprene Measurements From Space: Detecting Daily Variability at High Resolution, *J. Geophys. Res. Atmospheres*, 2022, **127**, e2021JD036181.

42 K. C. Wells and D. B. Millet, ROCR Isoprene Retrievals from the CrIS Satellite Sensor, *Univ. Minn. Data Repos.*, DOI:10.13020/5n0j-wx73.

43 US Environmental Protection Agency (EPA), Air Data, https://www.epa.gov/outdoor-air-quality-data (accessed 10 July 2023).

44 IMPROVE, Federal Land Manager Environmental Database (FED), http://views.cira.colostate.edu/fed/ (accessed 10 July 2023).

45 European Space Agency (ESA), Sentinel-5P TROPOMI Tropospheric NO2 1-Orbit L2 7km x 3.5km V1, *NASA Goddard Earth Sci. Data Inf. Serv. Cent. GES DISC*, DOI:10.5270/S5P-s4ljg54.

46 European Space Agency (ESA), Sentinel-5P TROPOMI Tropospheric Formaldehyde HCHO 1-Orbit L2 7km x 3.5km V1, *NASA Goddard Earth Sci. Data Inf. Serv. Cent. GES DISC*, DOI:10.5270/S5P-tjlxfd2.

47 K. R. Travis, D. J. Jacob, J. A. Fisher, P. S. Kim, E. A. Marais, L. Zhu, K. Yu, C. C. Miller, R.

M. Yantosca, M. P. Sulprizio, A. M. Thompson, P. O. Wennberg, J. D. Crounse, J. M. St. Clair, R. C. Cohen, J. L. Laughner, J. E. Dibb, S. R. Hall, K. Ullmann, G. M. Wolfe, I. B. Pollack, J. Peischl, J. A. Neuman and X. Zhou, Why do models overestimate surface ozone in the Southeast United States?, *Atmospheric Chem. Phys.*, 2016, **16**, 13561–13577.

48 C. Wiedinmyer, J. Greenberg, A. Guenther, B. Hopkins, K. Baker, C. Geron, P. I. Palmer, B. P. Long, J. R. Turner, G. Pétron, P. Harley, T. E. Pierce, B. Lamb, H. Westberg, W. Baugh, M. Koerber and M. Janssen, Ozarks Isoprene Experiment (OZIE): Measurements and modeling of the “isoprene volcano”, *J. Geophys. Res. Atmospheres*, DOI:10.1029/2005JD005800.

49 G. McFiggans, T. F. Mentel, J. Wildt, I. Pullinen, S. Kang, E. Kleist, S. Schmitt, M. Springer, R. Tillmann, C. Wu, D. Zhao, M. Hallquist, C. Faxon, M. Le Breton, Å. M. Hallquist, D. Simpson, R. Bergström, M. E. Jenkin, M. Ehn, J. A. Thornton, M. R. Alfarra, T. J. Bannan, C. J. Percival, M. Priestley, D. Topping and A. Kiendler-Scharr, Secondary organic aerosol reduced by mixture of atmospheric vapours, *Nature*, 2019, **565**, 587–593.

50 Smithsonian Astrophysical Observatory and National Aeronautics and Space Administration, Tropospheric Emissions: Monitoring of Pollution (TEMPO), https://tempo.si.edu (accessed 10 July 2023).

Supplementary Information

Implementation and Evaluation of the Automated Model Reduction (AMORE) Version 1.1 Isoprene Oxidation Mechanism in GEOS-Chem

Benjamin Yang,[*ab] Forwood C. Wiser,[c] V. Faye McNeill,[bc] Arlene M. Fiore,[d] Madankui Tao,[abd] Daven K. Henze,[e] Siddhartha Sen,[f] and Daniel M. Westervelt[*a]

* Corresponding authors

[a] Lamont-Doherty Earth Observatory, Columbia University, Palisades, NY, USA
E-mail: benjamin.yang@columbia.edu, danielmw@ldeo.columbia.edu

[b] Department of Earth and Environmental Sciences, Columbia University, New York, NY, USA

[c] Department of Chemical Engineering, Columbia University, New York, NY, USA

[d] Department of Earth, Atmospheric, and Planetary Sciences, Massachusetts Institute of Technology, Cambridge, MA, USA

[e] Department of Mechanical Engineering, University of Colorado Boulder, Boulder, CO, USA

[f] Microsoft Research, New York, NY, USA

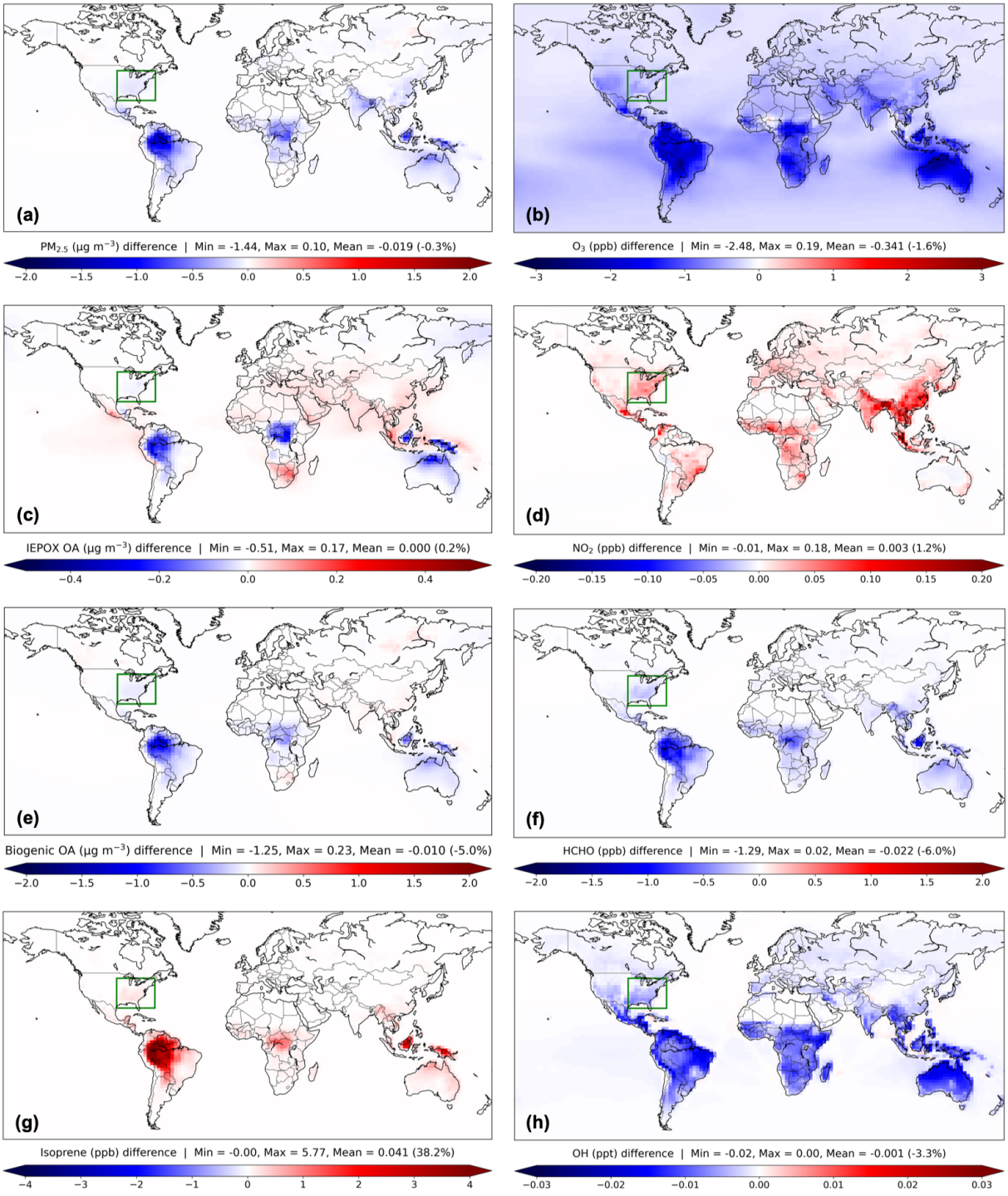

Figure S1. Global difference (AMORE - BASE) maps of 2° x 2.5° GEOS-Chem simulated (a) $PM_{2.5}$ (μg m^{-3}), (b) O_3 (ppb), (c) aerosol-phase IEPOX (μg m^{-3}), (d) NO_2 (ppb), (e) biogenic OA (μg m^{-3}), (f) HCHO (ppb), (g) isoprene (ppb), and (h) OH (ppt) averaged over June 2018 – May 2019. Blue and red denote grid boxes where concentrations were lower and higher, respectively, in AMORE than BASE. Minimum, maximum, and mean global differences are shown above the color bars. Our primary study area is the eastern US (green boxes).

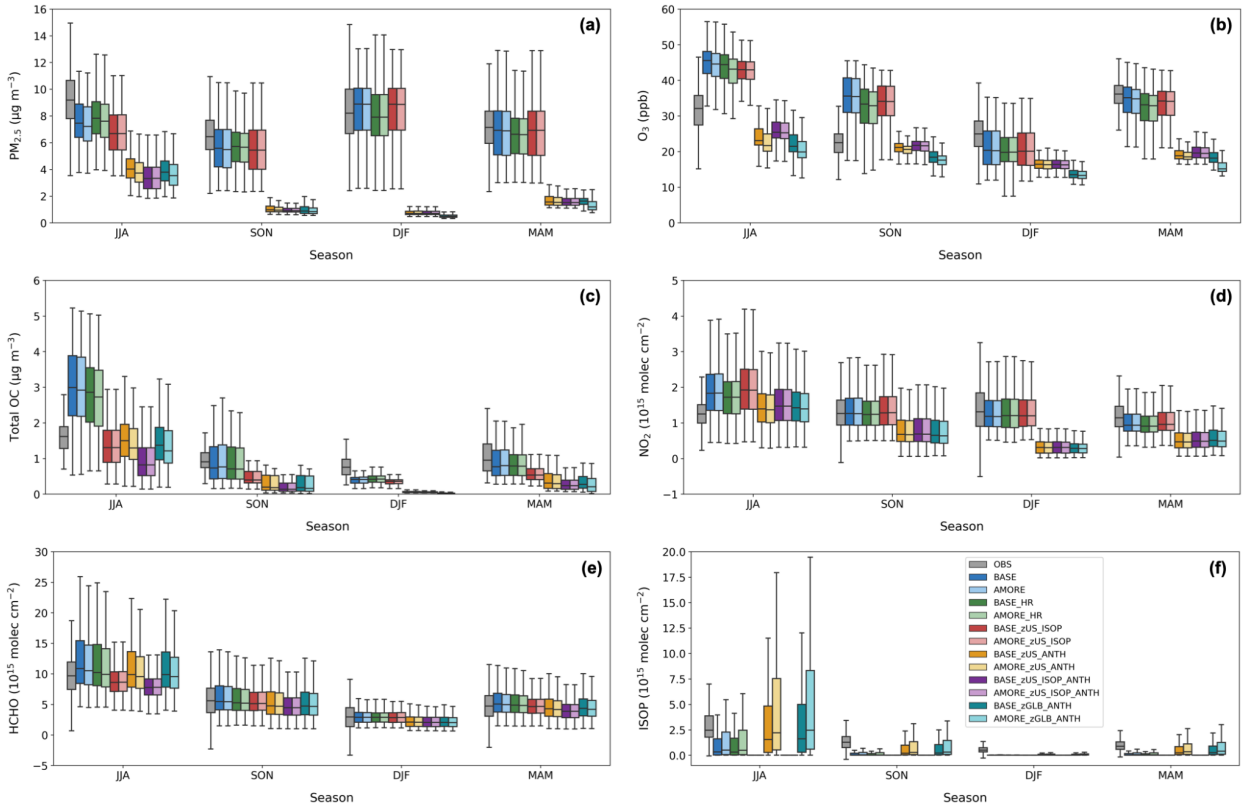

Figure S2. Seasonal distributions of monthly (a) $PM_{2.5}$ (μg m^{-3}), (b) O_3 (ppb), (c) total OC (μg m^{-3}), (d) NO_2 tropospheric VCD (10^{15} molecules cm^{-2}), (e) HCHO tropospheric VCD (10^{15} molecules cm^{-2}), and (f) isoprene total VCD (10^{15} molecules cm^{-2}) at AQS/IMPROVE sites (a-c) or TROPOMI/CrIS grid boxes (d-f) across the EUS for observations (gray box plots) versus all 12 GEOS-Chem simulations (other box plots). BASE (dark colors) and AMORE (light colors) mechanism sensitivity simulations are paired. The order of seasons is summer (JJA), fall (SON), winter (DJF), and spring (MAM). Each box plot shows the standard interquartile range (IQR) from the 25th (Q1) to 75th (Q3) percentiles, with whiskers extending to Q1 - (1.5 × IQR) and Q3 + (1.5 × IQR).

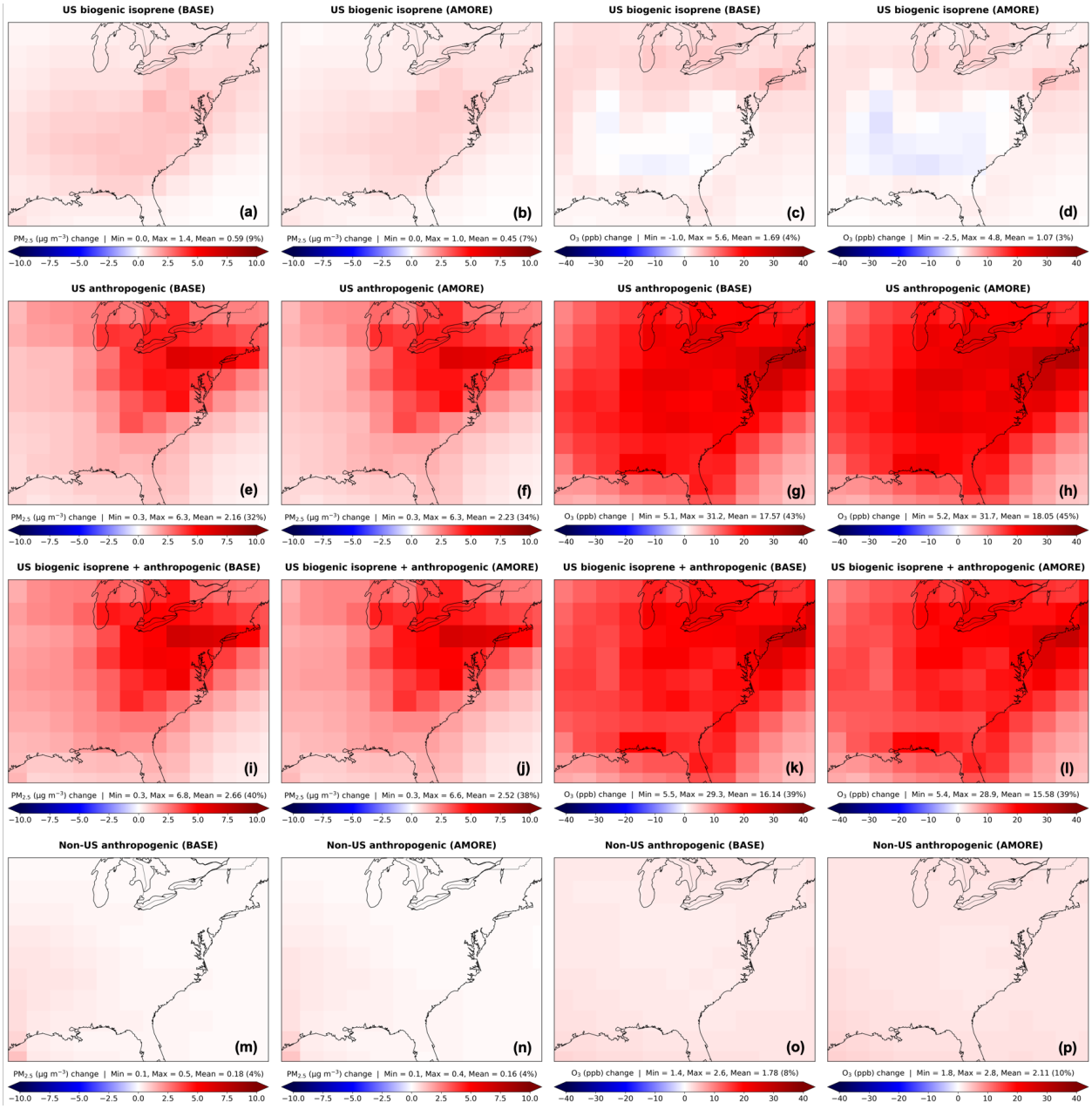

Figure S3. EUS maps of summer average (June–August 2018) sensitivities of $PM_{2.5}$ (μg m^{-3}, columns 1-2) and O_3 (ppb, columns 3-4) to "adding in" different emissions across the EUS domain at 2° x 2.5° resolution. Concentration changes are BASE minus BASE zero emissions or AMORE minus AMORE zero emissions (rows 1-3). Non-US anthropogenic (row 4) represents zUS_ANTH minus zGLB_ANTH.